Int J Adv Manuf Technol (2013) 69:2373–2386
DOI 10.1007/s00170-013-5184-6

ORIGINAL ARTICLE

Angular distortion analysis of the multipass welding process on combined joint types using thermo-elastic–plastic FEM with experimental validation

Robert Ngendang Lidam · Yupiter H. P. Manurung · Esa Haruman · M. Ridhwan Redza · M. Ridzwan Rahim · M. Shahar Sulaiman · M. Yusof Zakaria · Ghalib Tham · Sunhaji K. Abas · Chan Yin Chau

Received: 19 March 2012 / Accepted: 4 July 2013 / Published online: 3 August 2013

Abstract In this research, the capability of the multipass welding advisor (MWA) is to be evaluated in analyzing the angular distortion that is induced by gas metal arc welding (GMAW) process used to join a combination of butt and T-joint with thickness of 9 mm. The MWA in SysWeld 2010 is applied to develop and compare 2D/3D finite element analysis (FEA) based on the thermal elastic–plastic approach with low manganese carbon steel S355J2G3 as parent and weld material. For this simulation, the heat source of GMAW follows the Goldak's double ellipsoid model that is available within the FEA code. Detailed procedures of MPA are presented throughout this study followed with a comparison between 2D and 3D results of distortion and computational time on the combined types. To validate the simulation results, a series of experiments was conducted on low carbon steel using robotic welding process, GMAW power source with shielding gas composition of Ar (80 %)/CO_2 (20 %), and both-sided clamping method. It was established that the results of 3D simulation and experiments showed acceptable accuracy, while 2D results offers a fast solution analysis time in estimating distortion trend.

R. N. Lidam · Y. H. P. Manurung (✉) · M. R. Redza · M. R. Rahim · M. S. Sulaiman · M. Y. Zakaria · G. Tham · S. K. Abas
Faculty of Mechanical Engineering, Universiti Teknologi MARA, 40450 Shah Alam, Selangor, Malaysia
e-mail: yupiter.manurung@salam.uitm.edu.my

E. Haruman
Bakrie University, Jakarta, Indonesia

C. Y. Chau
ESI Group, South East Asia, Selangor, Malaysia

Keywords Multipass welding · Angular distortion · Thermo-elastic–plastic FEM · SYSWELD · Multipass welding advisor

1 Introduction

Welding is extensively used as a principal method of fabricating and assembling numerous metal products in shipbuilding, construction, aviation, and automotive industries. One of the popular arc welding processes is gas metal arc welding (GMAW) that has been applied in a wide range of plate thicknesses due to its ease and relatively high productivity. Welding is considered one of the most efficient, dependable, and economical means of fabrication to join metals permanently. However, distortion emerges as a result of the welding process which adversely affects the dimensional accuracy and esthetic value, which in turn can lead to expensive remedial work, which increases the overall fabrication costs. Distortion in a welded part occurs due to nonuniform expansion and contraction of the weld metal and adjacent parent metals caused by complex temperature changes during the welding process. In addition, the distortion resulting from the welding process can also induce residual stress, which may significantly influence the structural performance of the welded structure [1].

Multipass butt and T-joints are widely used in ship panel fabrication, such as in the hull section of the ship structure. To minimize production cost, it is important to understand the distortion behavior of multipass welding, which can be predicted by using simulation approach. The computational analysis can be used to achieve good welding quality and effective welding design in shipbuilding fabrication.

To the author's knowledge, there have been few attempts in the prediction of welding distortion with multipass techniques. Most of the reviewed publications focused on single-

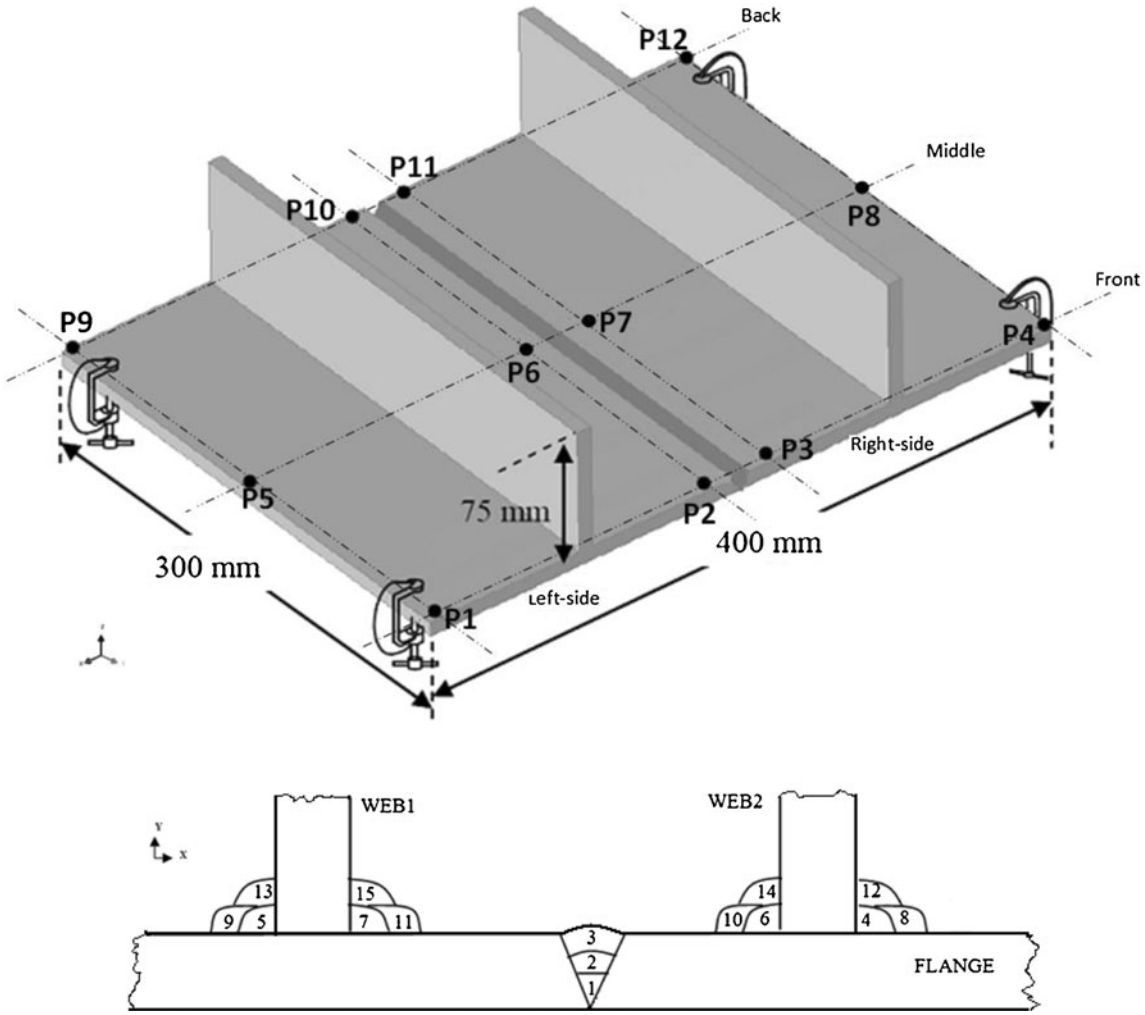

Fig. 1 Combined butt and T-joint geometry and welding sequences

pass welding. The purpose of this study is to analyze the angular distortion induced by multipass GMAW on combined butt and T-joint using simulation and experiment. The specimen was modeled and simulated based on thermal elastic–plastic 2D/3D finite element method (FEM) using the already established software SYSWELD 2010. This FEA software is known to be widely used to simulate weld-induced distortion, especially for single-pass process. In addition, the step-by-step procedures of the simulation process using multipass welding advisor in SYSWELD will be explained and presented as well.

Further, the simulation results were validated using a series of experiments which was conducted by means of fully automated robotic welding process (ABB IRB 2400/16) with digital GMAW power source (Kemppi Pro Evolution MXE) and shielding gas composition of Ar/CO_2 (80/20). The specimen made of low carbon material was clamped on both sides during the experimental investigation. Figure 1 shows the geometry, clamping position, welding sequences, and the location (P_i) where distortions are measured.

2 Principles of welding distortion simulation using FEM

Prediction of welding distortion using numerical methods through computer simulation has gained popularity in recent years. Among other classical numerical solutions, the FEM

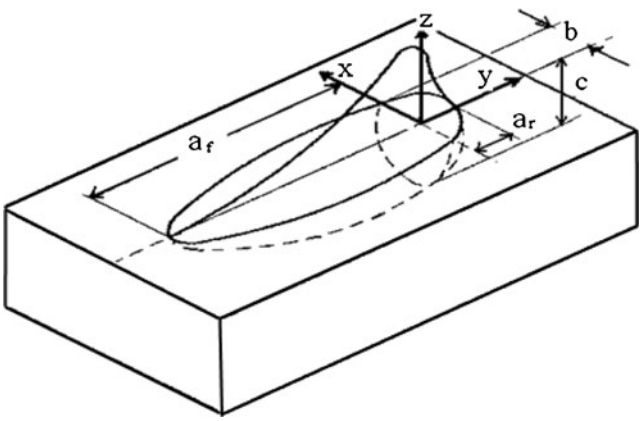

Fig. 2 Goldak's double ellipsoidal model

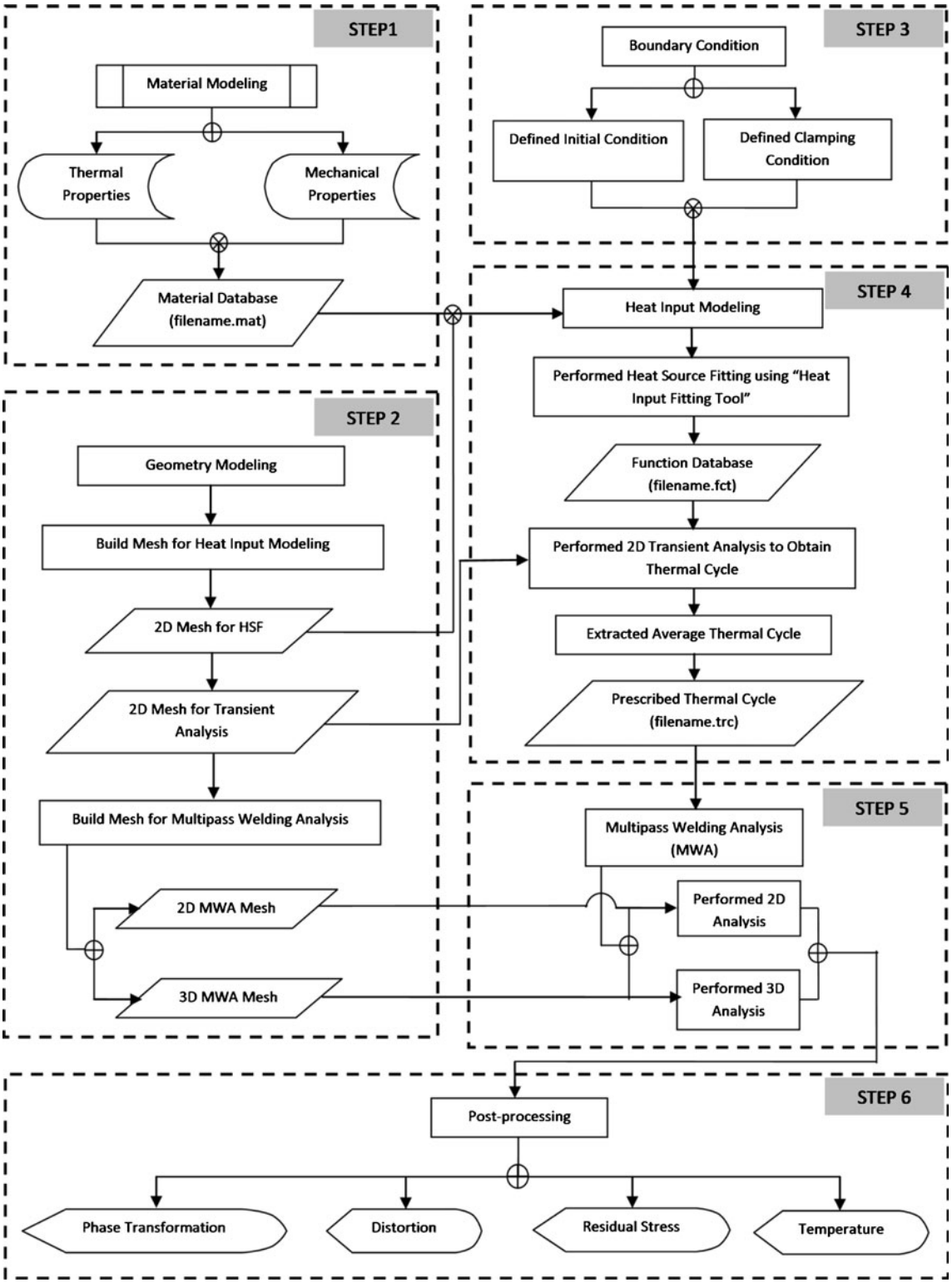

Fig. 3 Simulation procedures of multipass welding advisor in SYSWELD2010

is the most common approach used to model and analyze the welding process, with some others use either finite different method [2] or finite volume method [3].

FEM simulation is known as a complementary tool with respect to experimental techniques applied to determine the behavior and interactions between complex physical phenomena

Table 1 Chemical composition, mechanical, and thermal properties of low carbon steel

Elements		C	Si	Mn	S	P	Cr	Ni
Composition in wt%	S355J2G3 in SYSWELD	0.180	1.600	0.550	0.035	0.035	0	0
	Low carbon steel for experiment	0.186	0.146	0.011	0.001	0.001	0.035	0.032
Properties			Values					
Young's modulus (GPa)			210 (at 20 °C)					
Minimum yield strength (MPa)			355					
Poisson's ratio, ν			0.33					
Solidus temperature, TS (°C)			1,404					
Liquidus temperature, TL (°C)			1,505					

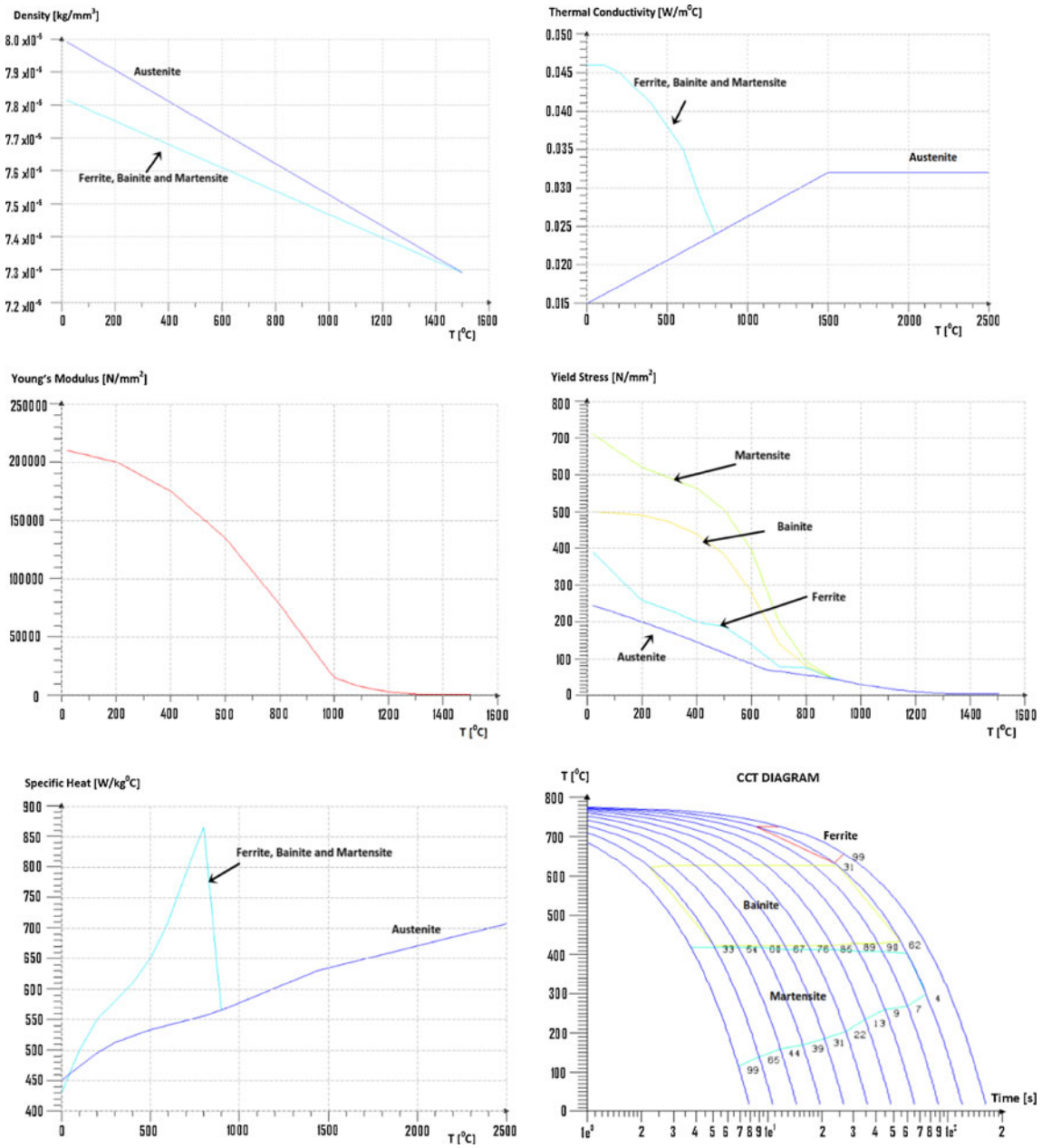

Fig. 4 Physical and mechanical properties of S355J2G3 low alloy manganese carbon steel (SYSWELD)

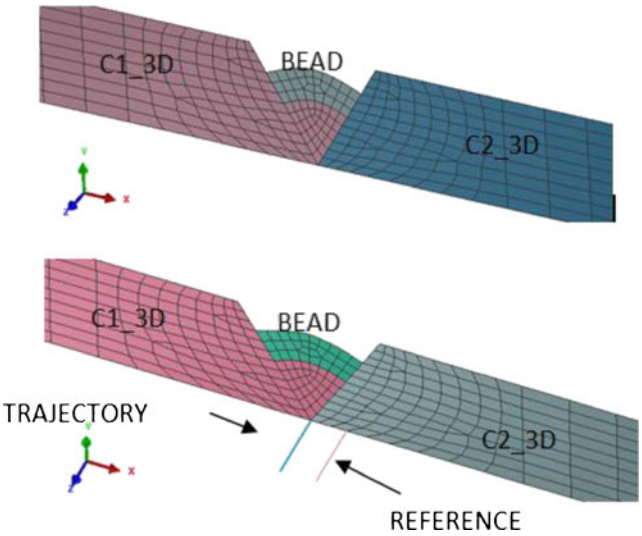

Fig. 5 2D local butt joint mesh model for heat source fitting (*top*) and thermal cycle extraction (*below*)

in the welding process. Various FEM have been rapidly developed and among most frequently used are thermo-elastic–plastic (TEP) [4–13], linear thermo-elastic shrinkage (LTES) [14, 15], inherent strain [16–18], and local–global approach (LGA) [19–21].

The LTES approach is based on linear elastic finite element modeling and does not take into account the transient temperature and physical properties of material, while the inherent strain method is based on plastic strain theory. Both methods are commonly used to calculate welding deformation in large structures. On the other hand, LGA uses a local 3D approach for the precise modeling of the complex physical phenomena induced by welding and then transferred the result into a macro element which is used in a global shell model for calculating distortion. These methods are developed based on achieving shorter computational time. However, simulation of the welding process is not easy, since it involves the interaction of thermal, mechanical, and metallurgical phenomena [4]. The TEP approach is the most popular method and has been applied by many researchers in predicting the welding distortion numerically because this method does take into account the transient temperature history and the material properties.

For the fusion welding process, the dedicated FE software package SYSWELD can perform (1) the thermal and metallurgical calculations, which can couple temperatures and phase proportions, and (2) the mechanical calculations, which depend not only on temperature but also on the element's metallurgical history.

During welding, a high nonuniform temperature field is generated. An accurate thermal analysis with appropriate boundary condition is of paramount importance for the determination of the realistic temperature profile to simulate the process [12]. The heat is transferred in welding mainly by conduction and lost to surrounding by convection and radiation [22]. Heat diffusion by conduction is based on Fourier's Law [23], where heat flux (q in W/m^2) flows from hot to cooler regions and is linearly dependent on the temperature

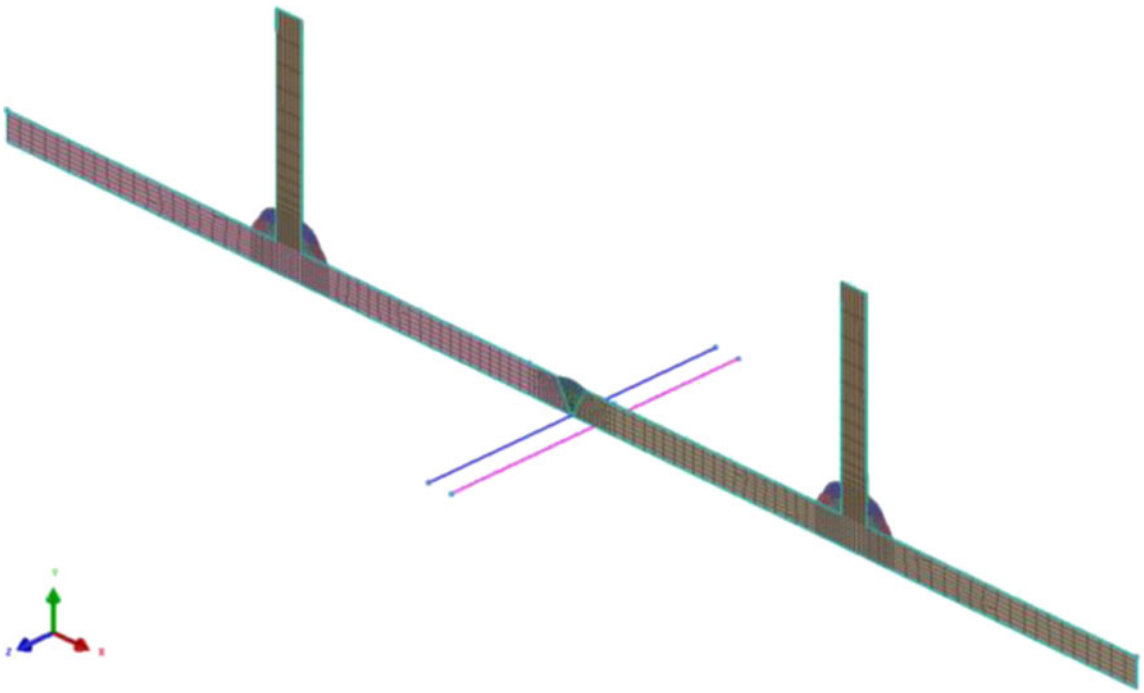

Fig. 6 2D global mesh model for 2D multipass analysis

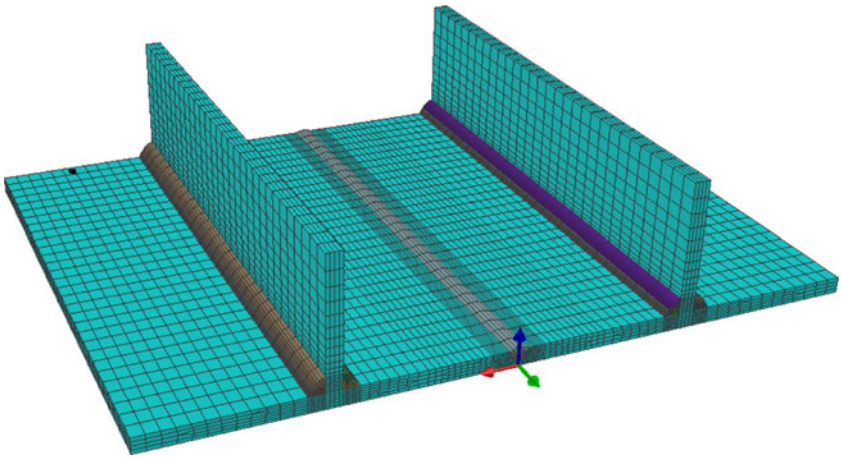

Fig. 7 3D global mesh model for 3D multipass analysis

gradient. The governing equation for nonlinear transient heat conduction is as follows:

$$\rho c_p \frac{\partial T}{\partial t} = \frac{\partial}{\partial x}\left(k(T)\frac{\partial T}{\partial x}\right) + \frac{\partial}{\partial y}\left(k(T)\frac{\partial T}{\partial y}\right) + \frac{\partial}{\partial z}\left(k(T)\frac{\partial T}{\partial z}\right) + Q \quad (1)$$

Where T, ρ, c_p, and Q are temperature (in Kelvin), density (in kilograms per cubic meter), specific heat (in Joule per kilogram Kelvin), and internal heat source (in Watts per cubic meter) respectively. The product of $\rho \times c_p$ reflects the capacity of the material to store energy. When heat diffusion is treated with an enthalpy-based formulation to solve the problem in liquid and solid domains, the general heat transfer equation becomes [24]:

$$\rho c_p \frac{\partial H}{\partial t} = \frac{\partial}{\partial x}\left(\frac{k(T)}{\rho c_p}\frac{\partial H}{\partial x}\right) + \frac{\partial}{\partial y}\left(\frac{k(T)}{\rho c_p}\frac{\partial H}{\partial y}\right) + \frac{\partial}{\partial z}\left(\frac{k(T)}{\rho c_p}\frac{\partial H}{\partial z}\right) + Q \quad (2)$$

with

$$H_1 - H_2 = \int_{T_1}^{T_2} \rho c_p \, dT \quad (3)$$

Where H is enthalpy, T_1 and T_2 are the initial and final time temperatures.

The total heat input or internal heat source (Q in Watts per cubic meter) in arc welding is the product of arc power (VI in Watts) and process efficiency (η).

$$Q = \eta VI \quad (4)$$

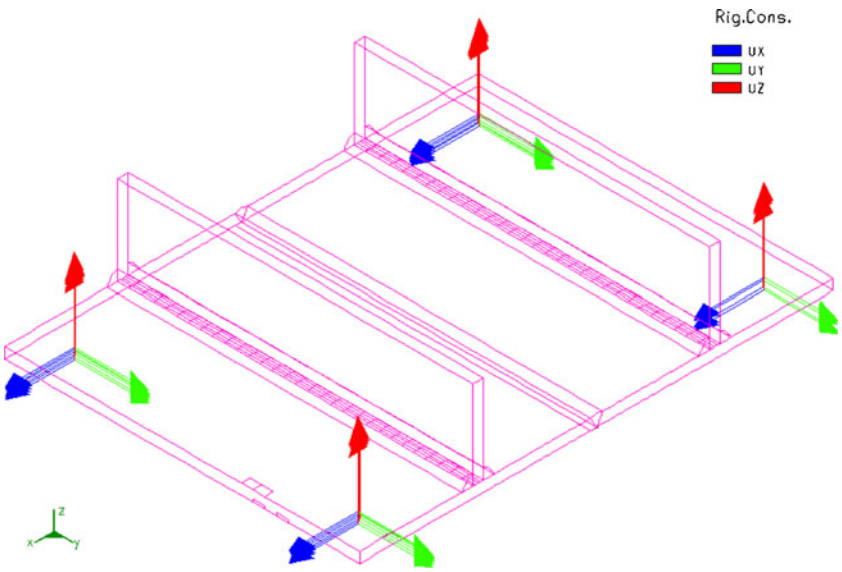

Fig. 8 Clamping model of welding simulation

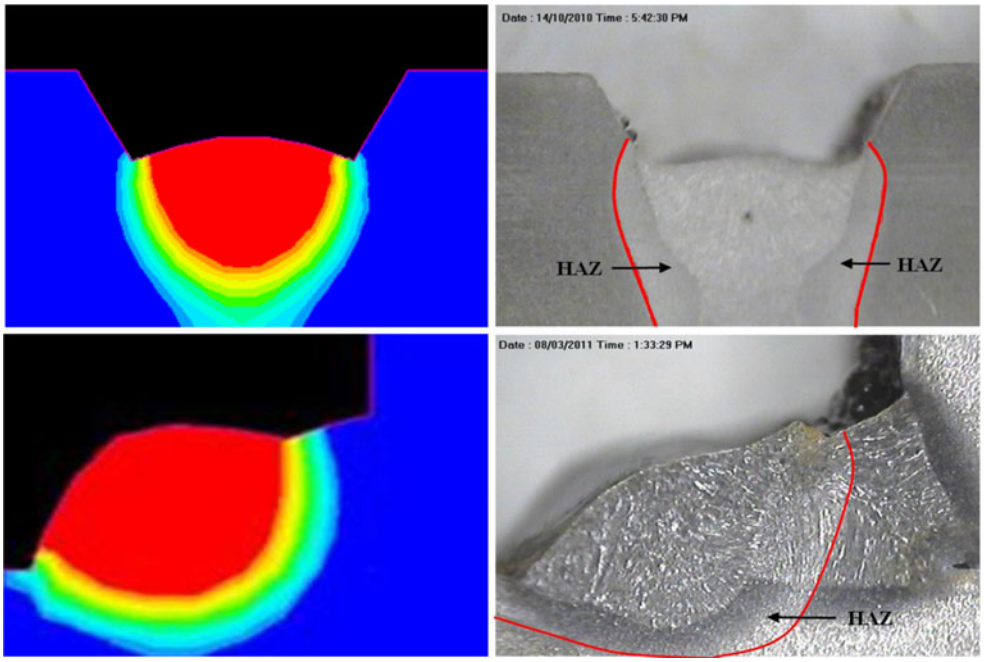

Fig. 9 Heat source profile for butt and T-joint from SYSWELD and macrograph example

For GMAW, the heat source efficiency varies between 65 and 85 % [22]. For many arc welds, a good approximation of heat input (Q) is achieved by using the double ellipsoidal shape as proposed by Goldak and Akhlaghi [25] using the following equation:

$$q_{f,r}(x,y,z,t) = \frac{6\sqrt{3} f_{f,r} Q}{abc\pi\sqrt{\pi}} e^{\frac{-3x^2}{a^2}} e^{\frac{-3y^2}{b^2}} e^{\frac{-3[z+v(\tau-t)]^2}{c^2}} \quad (5)$$

In this model, f_f and f_r are the fractions of the heat deposited in the front and rear quadrant, respectively, where f_f+-f_r=2, a,b,c are the dimension parameters of the heat source, v is welding velocity, t is time, and τ is lag factor of the heat deposited at t=0. Figure 2 shows the proposed Goldak's double ellipsoid model.

Generally, the thermal boundary conditions consist of heat flux density imposed on the side wall and imposed coefficient of thermal change. In this present study, only coefficient of thermal exchange which consists of convection and radiation losses is considered. The overall thermal boundary condition can be defined as follows:

$$Q - h_{conv}(T_s - T_\infty) - \varepsilon\sigma(T_s - T_\infty) = 0 \quad (6)$$

Where $T_s - T_\infty$ is the temperature difference between the given body temperature (T_s) and its surrounding (T_∞). h_{conv}, σ and ε are the convection heat transfer coefficient, Stefan Boltzmann's constant, and thermal emissivity, respectively.

The calculation takes into account phase transformation, and in the case of steels, a distinction is generally made between diffusion type phase and martensitic type transformation [26].

Table 2 Heat source parameters

Parameter		Butt joint	T-joint
Maximal front source intensity, Qf (W/mm3)		21.46	20.77
Maximal rear source intensity, Qr (W/mm3)		32.19	27.63
Gaussian parameter	af (mm)	3	3
	ar (mm)	7	7
	b (mm)	2	2
	c (mm)	3	3
Initial location of source center	xo (mm)	0	6
	yo (mm)	0	0
	zo (mm)	6	2
Angle of torch, Ay (deg)		0	45
Source displacement velocity,Vy(mm/s)		4	4
Power, P (Watts)		3,000	3,200

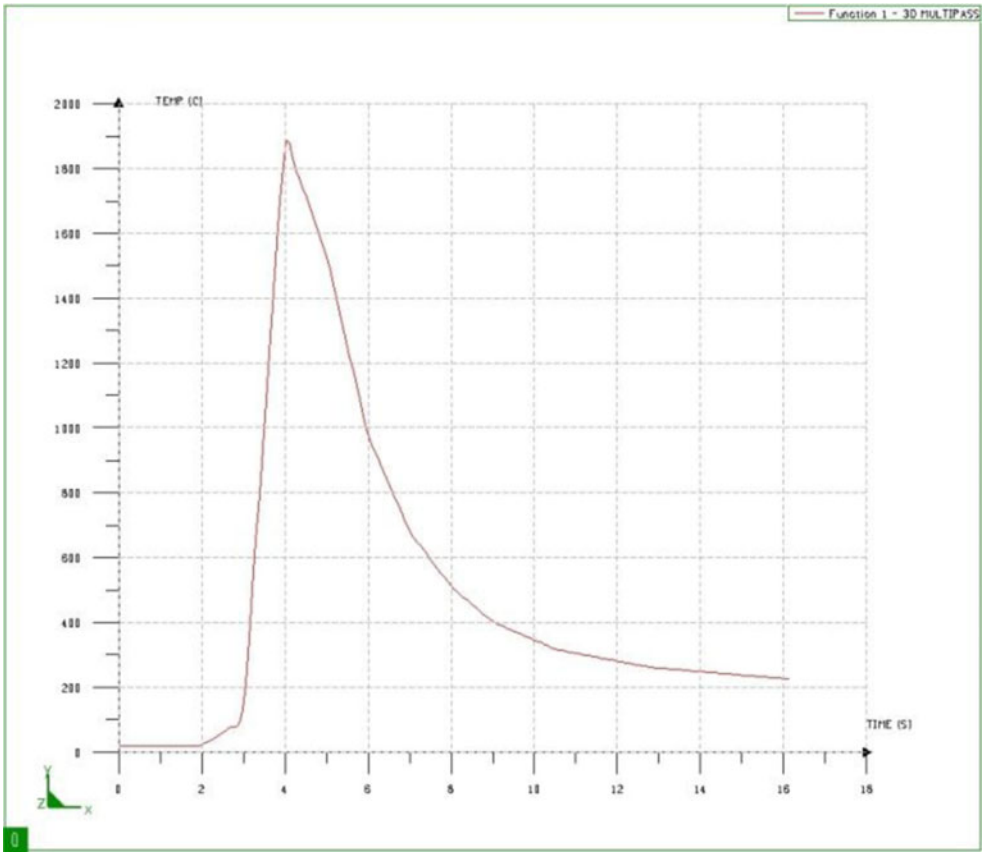

Fig. 10 Average thermal cycle of T-joint in the bead after modification

The diffusion type transformation is described by the generalized Leblond model (Johnson–Mehl–Avrami) for a transformation between two phases (1→2) and can be formed as follow:

$$\dot{p}_2 = n_{1\to 2}(T)\frac{\overline{p}_2(T)-p_2}{\tau_{1\to 2}(T)}\left(\ln\left(\frac{\overline{p}_2(T)}{\overline{p}_2(T)-p_2}\right)^{\frac{n_{1\to 2}(T)-1}{n_{1\to 2}(T)}}\right) \tag{7}$$

Where $\overline{p}$ represents the phase proportion obtained after an infinite time at temperature T, τ_R is a delay time, and n is an exponent associated with the reaction speed. For this transformation law, the required parameters are obtained from the continuous cooling transformation diagram [27].

The martensitic transformation depends on temperature alone and is described by the Koistinen–Marburger law as follows:-

$$p(T) = \overline{p}.(1-\exp(-\mathrm{b}.(\mathrm{Ms}\text{-}T))) \quad with \quad T \leq \mathrm{Ms} \tag{8}$$

In this case, $\overline{p}$ represents the proportion obtained at an infinitely low temperature which is frequently assimilated to 1. Ms and b characterize initial transformation temperature

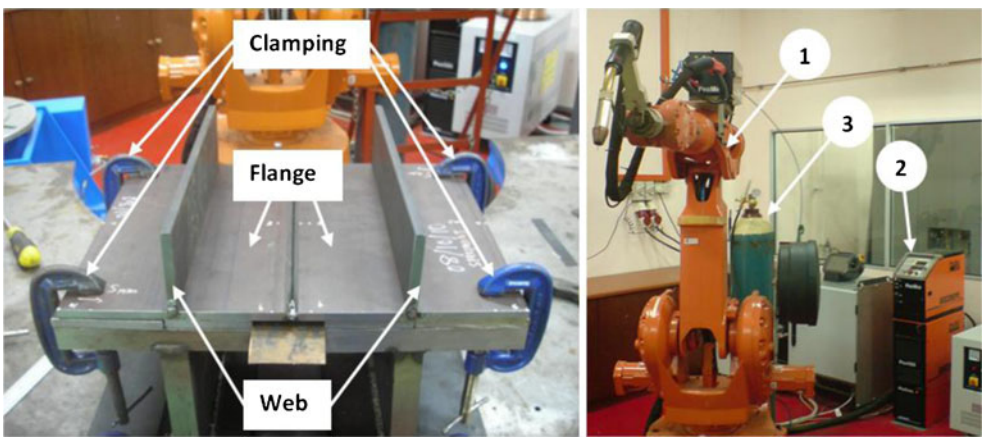

Fig. 11 Welding set-up and robotic welding apparatus: (*1*) ABB IRB 2400/16, (*2*) KEMMPI ProMIG 540 MXE, and (*3*) shielding gas (80 % Ar and 20 % CO_2)

Table 3 Welding parameters used in experiments

		Current (A)	Voltage (V)	Travel speed (mm/s)
Butt joint	1st pass	115–157	20	6
	2nd pass	115–155		4
	3rd pass	115–162		2
T-joint	1st pass	115–152		6
	2nd pass	115–151		5
	3rd pass	115–155		4

and evolution of the transformation process according to temperature, respectively.

For mechanical analysis, to relate the stress and strain, Hooke's Law is used for isotropic material. The plastic flow rule is associated with von Mises criterion. The equivalent stress is given as follow:

$$\sigma_\nu = \sqrt{\frac{1}{2}\left[(\sigma_1-\sigma_2)^2 + (\sigma_2-\sigma_3)^2 + (\sigma_3-\sigma_1)^2\right]} \quad (9)$$

Where σ_1, σ_2, and σ_3 are the principal stresses coupled to strain hardening rule, and the total strain rate ($\Delta\varepsilon_{ij}^{total}$) can be defined as a sum of elastic strain rate ($\Delta\varepsilon_{ij}^{e}$), plastic strain rate ($\Delta\varepsilon_{ij}^{p}$), transformation plastic strain rate ($\Delta\varepsilon_{ij}^{tp}$), and thermo-metallurgical strain ($\Delta\varepsilon_{ij}^{th}$) such that [28] :

$$\Delta\varepsilon_{ij}^{total} = \Delta\varepsilon_{ij}^{e} + \Delta\varepsilon_{ij}^{p} + \Delta\varepsilon_{ij}^{tp} + \Delta\varepsilon_{ij}^{th} \quad (10)$$

3 Simulation procedures of multipass welding advisor in SYSWELD 2010

In general, these simulation processes involve three major phases: modeling, analyzing, and post-processing. Material, geometry, and heat input modeling belong to the first phase. Transient analysis was conducted to solve thermal problem to obtain temperature history which is later used to solve mechanical problem. Finally, post-processing was performed to display the result obtained from the analysis.

SYSWELD can simulate both single-pass and multipass welding process. The standard welding simulation methods (moving heat source) only can be applied on single-pass welding process, but cannot be applied on multipass welding process due to large computational files to be managed and disk space requirement. In order to deal with such complex simulations in an efficient manner, SYSWELD provides a management tool called the "multipass welding advisor" which includes automatic tools and methods to ease multipass welding simulation. The multipass welding process involves six steps as shown in Fig. 3.

Step 1 Defining material properties. The material used in this present study is low alloy carbon manganese steel (S355J2G3). SYSWELD enables users to use the predefined material properties data or develop the thermo-metallurgical and mechanical behavior data for the simulation purpose, which requires extensive research. SYSWELD provides a material database for S355J2G3, and its chemical composition is shown in Table 1. In welding computations, thermal material properties are highly nonlinear and depend on the temperature and phase-dependent physical properties of low alloyed carbon manganese steel given in Fig. 4.

Step 2 Developing mesh of geometry model. The customized geometry model was developed using Visual Mesh 6.5, which is a powerful design and meshing tool. A file (filename_DATA1000.ASC) created in Visual Mesh is imported into SYSWELD used as input data in simulation. There are four mesh

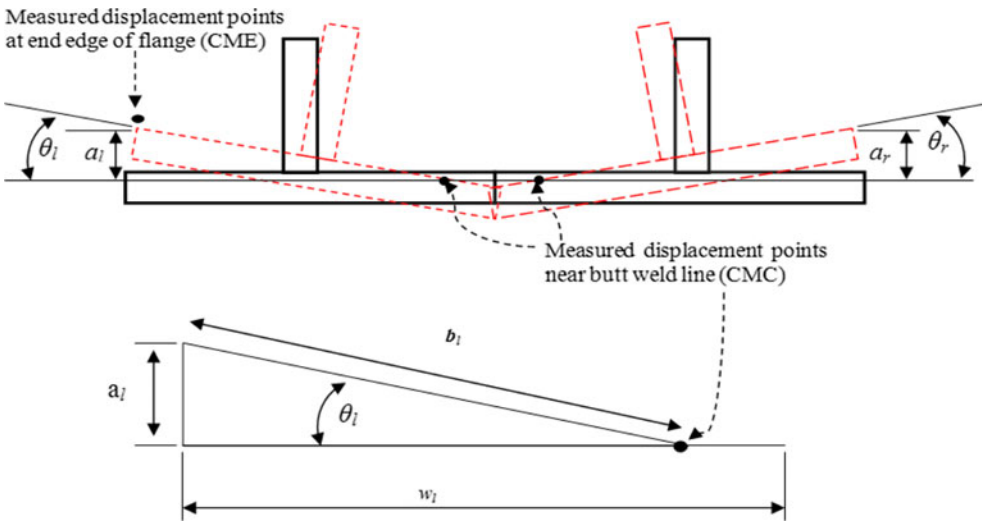

Fig. 12 Schematic diagram for calculating angular distortion

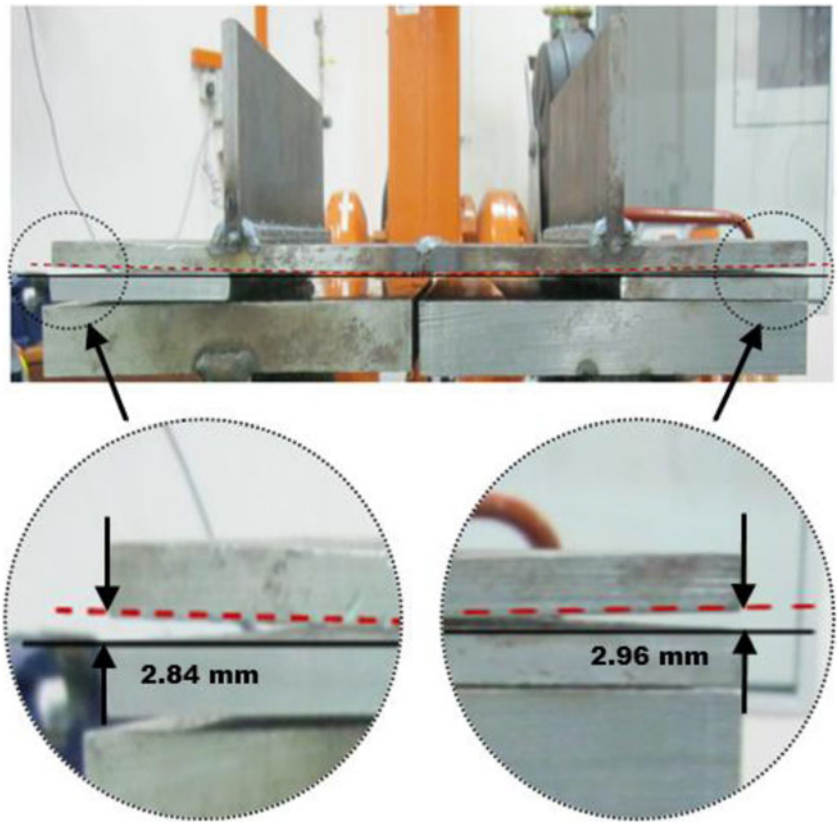

Fig. 13 Final angular distortion induced by welding process

models required in the multipass welding simulation namely: (1) 2D local mesh for heat source fitting, (2) 2D local mesh analysis for thermal cycle extraction, (3) 2D global mesh for 2D multipass analysis, and (4) 3D global mesh geometry for 3D multipass analysis. The mesh models are shown in Figs. 5, 6, and 7, respectively.

Step 3 Defining and setting boundary condition. Two types of boundary conditions (thermal and mechanical) are to be defined. While, as described earlier, thermal boundary conditions are caused by convection and radiation losses, the mechanical boundary conditions are defined by the clamping arrangement, which was modeled as being rigid, shown in Fig. 8.

Step 4 Modeling heat input. In this simulation method, the correct heat input selection and modeling are detrimental to the outcome. It is very important to understand the concept of heat input being employed. As mentioned previously, the heat source was modeled using Goldak's double ellipsoidal model (see Fig. 2) to describe the heat input of welding process. The heat source function was created using heat input fitting tool available within SYSWELD, which allows the user to calibrate the heat source parameter and perform a steady-state thermal analysis of welding process. The analysis result provides the user with a temperature contour plot showing the predicted weld fusion zone, and, it is possible for the user to calibrate the heat source by comparing the predicted weld fusion zone with the actual macrograph from tested specimen. The heat model was calibrated by adjusting the Gaussian parameter until it generates a fusion zone that matches the macrograph shown as example in Fig. 9, for butt and T-joint. Table 2 shows the final double ellipsoid parameter. However, before this heat source can be used to simulate the multipass welding process, the average thermal cycle must be extracted and integrated into the function, in order to reduce the computation load. In order to obtain the thermal cycle for the multipass simulation, a 2D transient analysis should be performed. After completing the 2D analysis, the following steps need to be performed: (1) displaying the thermal curve in the bead via post-processing, (2) removing the portion where no temperature changes occur, and (3) extracting the average thermal curve. The extracted curve was exported and saved in the heat source function database with name “thermal_cycle.trc”. The average thermal cycle for T-joint after modification is shown in Fig. 10.

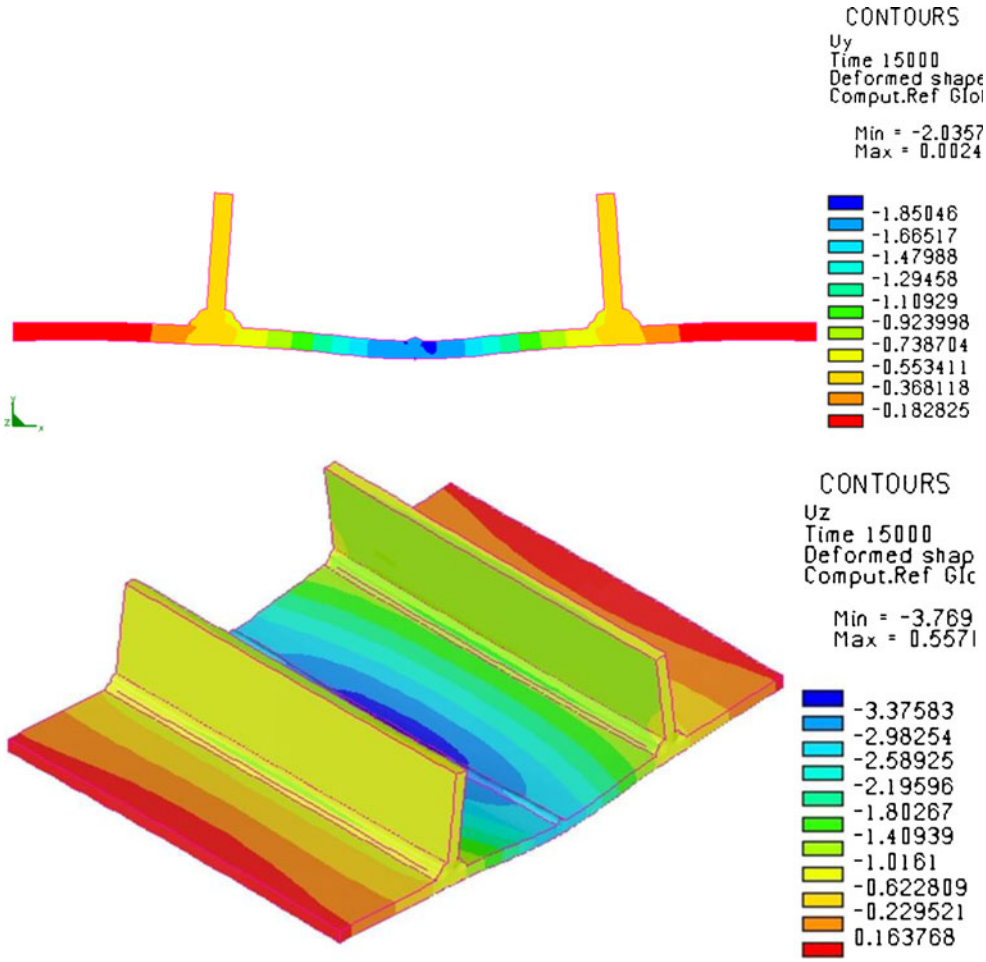

Fig. 14 Displacement of the combined joint types magnified by ×5 in 2D (*top*) and 3D (*below*) multipass analysis

Step 5 Performing the analysis. The input data is stored and saved using the "welding wizard," and then the project is solved using "multipass advisor". The 2D and 3D multipass analysis are performed separately using a similar step. The running simulation of 2D multipass analysis will take several minutes, while 3D multipass analysis requires several hours due to the massive number of elements and nodes.

Step 6 Visualizing and interpreting the result. This will be the final step of the simulation, where the result is visualized and interpreted. This will be done using the "post-processing" menu available in "welding advisor". Several methods are available to be used to interpret data such as contour or curve plot.

4 Experimental set-up and procedure

Experimental investigation was conducted on combined butt and T-joints using ABB IRB 2400/16 robotic system and Kemppi Pro Evolution MXE power source as shown in Fig. 11. Filler wire ER70S-6 (∅ 1.2 mm) and shielding gas composition Ar (80 %)/CO_2 (20 %) were used throughout this study. The process parameters used in this experiment are shown in Table 3. Prior to the welding process, the edge of the butt joint was prepared with a 60° included angle, while no edge preparation was made on T-joint, where the plates were positioned 90° to the flanges. The workpieces were tacked together using GTAW. The welding setup with clamping is shown in Fig. 11.

In these experimental tests, low carbon steel material has been used to predict the welding distortion. Mild steel has been widely used in many applications, combining good welding properties with good strength. Table 1 shows the chemical composition based on the international standards and the experimental results obtained using arc spark

Table 4 Angular distortions at the final time of the simulation in 2D analysis

	Left side of the flange	Right side of the flange
Displacement, a (in mm)	1.74	1.77
Angular distortion, θ (in deg)	0.54	0.55

Table 5 Angular distortions at the final time of the simulation in 3D analysis

Position relative to Y direction	Left side of the flange			Right side of the flange		
	a_l (mm)		θ_l (deg)	a_r (mm)		θ_r (deg)
Front	P1–P2	2.97	0.92	P4–P3	3.07	0.95
Middle	P5–P6	4.01	1.24	P8–P7	4.01	1.24
Back	P9–P10	3.02	0.94	P12–P11	3.07	0.95
$\overline{X}$	3.33		1.03	3.38		1.05

Table 6 Angular distortions at the final time of the experiment

Position relative to Y direction	Left side of the flange			Right side of the flange		
	a_l (mm)		θ_l (deg)	a_r (mm)		θ_r (deg)
Front	P1–P2	1.82	0.56	P4–P3	2.80	0.87
Middle	P5–P6	3.53	1.09	P8–P7	3.25	1.01
Back	P9–P10	3.16	0.98	P12–P11	2.82	0.87
$\overline{X}$	2.84		0.88	2.96		0.92

emission spectrometer with pure Argon 99.9 % and its software Spark Analyzer MX. The mechanical and thermal properties are also presented.

The distortion was measured using a coordinate measuring machine Mitotuyo 707. The measurement was conducted prior to and after the welding process on 12 selected points, as shown in Fig. 1, identified by the letter P_i.

5 Results and discussion

The angular displacement of the flange of the combined butt and T-joint perpendicular to the weld bead in the Uz direction was calculated based on the schematic diagram in Fig. 12, using the following equation:

$$\theta_{l,r} = \sin^{-1}\left(\frac{a_{l,r}}{b_{l,r}}\right) \tag{11}$$

Where θ is the resulting angular distortion, a is deflection measured at the edge of the flange (CME), b is the length from CME to the coordinate measured near center of the flange (CMC), w is half the flange width, and the distance of CMC to the center of the flange is fixed at 15 mm. Therefore, $b_{l,r}$=185 mm. A similar way to calculate angular distortion can be found in [29].

The distortion from the experiment is clearly shown in Fig. 13, with the flange were distorted in the Uz direction. For the simulation study, Fig. 14 shows the displacement of the combined butt and T-joint (magnified by ×5), respectively, in 2D and 3D multipass analysis, while presented in Tables 4,

Table 7 Comparison of the average result of angular distortion

Sequences	Position	Experiment	2D analysis		3D analysis	
		Angular distortion	Angular distortion	Percentage error (%)	Angular distortion	Percentage Error (%)
Outside to inside	Left side of the flange	0.88 % 2.84 mm	0.54 % 1.74 mm	38.6	1.03 % 3.33 mm	17.0
	Right side of the flange	0.92 % 2.96 mm	0.55 % 1.77 mm	40.2	1.05 % 3.38 mm	14.1

5, and 6 are the calculated angular distortions at the final time of the simulation for 2D, 3D, and experimental analysis, respectively. The comparison of the average result of angular distortion in 2D, 3D analyses, and experiment are presented in Table 7.

It can be seen from Tables 4, 5, and 6 that, at first, the relative differences of angular distortion between right to left side are approximately 1.72 % (2D), 1.50 % (3D), and 4.22 % (experiment). Although it shows that the first welded side had more angular distortion than the later welded one, it can be considered as not having significant difference. The reason of having bigger distortion could be due to the heat distribution which began and continuously overlapped at the right side. Secondly, the middle section exhibits the biggest angular distortion followed by the back and front section. Third, in comparison to experiment results shown in Table 7, the 3D simulation indicates better result agreement than 2D.

6 Conclusion and further recommendation

A study was conducted on the angular distortion in the multipass GMAW process on combined butt and T-joint using FE methods. FE software package SYSWELD and its multipass welding advisor were applied to simulate the welding process and to analyze the weld induced distortion. The analysis is calculated based on thermo-elastic–plastic approach which takes into account thermal, metallurgical, and mechanical properties. 2D and 3D analysis methods were performed, and both were validated with experimental investigation by comparing their results. Moreover, this paper also illustrates the step-by-step simulation process comprehensively. In general, there are six major steps to be conducted to analyze the distortion.

Based on the results, it can be concluded that (1) 3D FEM analysis shows better agreement compared to 2D FEM analysis; (2) computational time of 2D FEM was extremely faster (15 to 20 min) compared to 3D FEM (24 to 30 h); (3) steps for 2D FEM was shorter than 3D analysis; (4) both FEM methods (2D and3D) can carry out transient analysis; and (5) non-homogenous material, dimensional inconsistency, and fluctuating process parameters are such factors which can lead to the percentage error between idealized simulation and real experiments.

It can be generally summarized that FE method via SYSWELD is capable of simulating the multipass welding process and can be used to predict the angular distortion on combined butt and T-joints. From the analysis point of view, important information can be obtained which can be used prior to designing and as a planning tool before the actual welding process. It is recommended that welding sequence should be investigated further in order to know the effect of the sequence on the angular distortion of the complex structure.

Acknowledgment The authors would like to express their gratitude to the staff member of Welding Laboratory, Advanced Manufacturing Laboratory, and Advanced Manufacturing Technology Excellence Center (AMTEx) at the Faculty of Mechanical Engineering, Universiti Teknologi MARA (UiTM) for encouraging this study. This study is financially sponsored by E-Science MOSTI Project (no: 03-01-01-SF0355).

References

1. Mandal NR (2004) Welding and distortion control. Alpha Science international Ltd., UK
2. Al-Sa'ady MH, Abdul Sattar MA, Al-Khafagy LS (2011) Finite difference simulation of low carbon steel manual arc welding. Therm Sci 15(1):207–214
3. GA Taylor, M Hughes, N Strusevich, and K Pericleous (1999) "Finite volume methods applied to the computational modeling of welding phenomena," in Second International Conference on CFD in the Minerals and Process Industries, Melbourne, pp. 405–410.
4. Tsirkas SA, Papanikos P, Kermandis T (2003) Numerical simulation of the laser welding process in butt-joint specimens. J of Mater Process Technol 134:59–69
5. Bang H-S, Kim Y-P, Joo S-M, Kim J-M, Hwang W-S (2004) A study on the mechanical behaviors in welded parts by numerical simulation. Key Eng Mater 270–273:2371–2376
6. Kim J, Im S, Kim H-G (2005) Numerical implementation of thermo-elastic plastic constituitive equation in consideration of transformation plasticity in welding. Int J Plast 21:1383–1408
7. Mollicone P, Camilleri D, Gray TGF, Comlekci T (2006) Simple thermo-elastic–plastic models for welding distortion simulation. J Mater Process Technol 176:77–86
8. Zhang H, Zhang G, Cai C, Gao L, Wu L (2008) Fundamental studies on in-process controlling angular distortion in asymmetrical double-sided arc welding. J Mater Process Technol 205:214–223
9. Deng D (2009) FEM prediction of welding residual stress and distortion in carbon steel considering phase transformation effects. Mater Des 30:359–366
10. Deng D, Murakawa H (2008) Prediction of welding distortion and residual stress in a thin plate butt-welded joint. Computat Mater Sci 43:353–365
11. Long H, Gery D, Carlier A, Maropoulos PG (2009) prediction of welding distortion in butt joint of thin plates. Mater Design 30:4126–4135
12. Ullah Dar N, Ejaz Qureshi M, Hammouda MMI (2009) Analysis of weld-induced residual stresses and distortions in thin-walled cylinders. J Mech Sci Technol 23:1118–1131
13. Lidam RN et al (2011) Angular distortion analysis on multipassed welding of combined joint types using thermo-elastic–plastic FEM. Adv Mater Res 314–316:315–318
14. M. Slovacek, J. Kovarik, and J. Tejc (2009) "Using of welding virtual numerical simulation as the techinical support for industrial," in The 5th International scientific-professional conference SBW 2009 Robotization and Automation in Welding and other Techniques, Slavonski Brod, pp. 75–82
15. Lu Y, Wu P, Zeng J, Wu X (2010) Numerical simulation of welding distortion using shrinkage force approach and application. Advanced Materials Research 129–131:867–871
16. L Hao, C Jummei, and W Liangwu Welding distortion prediction of grab nether frame carbody bu FEM based on inherent strains, IIW Doc. X-1559-2004
17. Li H, Ren H (2007) Prediction of welding distortions of stainless steel ship. Key Eng Mater 284–349:373–376

18. Wang YX, Zhang P, Hou ZG, Li CZ (2008) Inherent strain method and thermal elastic–plastic analysis of welding deformation of a thin-wall beam. J Mech 24(4):301–309
19. Souloumiac B, Boitout F, Bergheau JM (2002) A new local–global approach for the modeling of welded steel component distortions. Math Model of Weld Phenom 6:573–590
20. Duan YG, Vincent Y, Boitout F, Leblond JB, Bergheau JM (2007) Prediction of welding residual distortions of large structures using a local/global approach. J Mech Sci Technol 21:1700–1706
21. J Bradac (2010) "Numerical analysis using in production of welded parts," Acta Technica Corviniensis Buletin of Engineering, pp. 89–93
22. Parmar RS (2005) Welding engineering and technology. Khanna Publishers, Delhi
23. Lewis RW, Nithiarasu P, Seetharamu KN (2004) Fundamental of the finite element for heat and fluid flow. John Wiley & Son Ltd., England
24. Lewis RW, Morgan K, Thomas HR, Seetharamu KN (1996) The finite element method in heat transfer analysis. John Wiley & Sons Ltd., England
25. Goldak JA, Mehdi A (2005) Computational welding mechanics. Springer Science + Business Media, Inc, USA
26. ESI Group (2010) SYSWELD 2010 Reference Manual. Digital Version
27. Seyffarth P, Meyer B, Scharff A (1992) Grosser Atlas Scheweiss-ZTU-Schaubilder. Deutscher Verlag fuer Schweisstechnik DVS-Verlag GmbH, Duesseldorf, German
28. ESI Group (2010) SYSWOLD 2010 Technical Description of Capabilities. Digital Version
29. Tso LT, Chin PF, Wei CY (August 2001) Analysis of residual stresses and distortion in T-joint filets welds. Int J of Press Vessel and Piping 78:523–538